Measurements of Higgs boson properties (mass, width and spin/CP) with the ATLAS detector

D. Muñoz Pérez, on behalf of the ATLAS Collaboration[a]
Instituto de Física Corpuscular (IFIC), University of Valencia-CSIC, Paterna, Spain

The most recent ATLAS measurements of the Higgs boson properties at the LHC are reviewed in this contribution. Highlights include the combination of the $H \to \gamma\gamma$ and $H \to ZZ^* \to 4\ell$ decay channels using both Run-1 and Run-2 data, which has yielded the most precise determination of the Higgs boson mass to date: $m_H = 125.11 \pm 0.11$ GeV. The total width of the Higgs boson, Γ_H, has been constrained through two complementary analyses: the first combining the on-shell $H \to ZZ^*$ and off-shell $H^* \to ZZ$ production, setting an observed (expected) 95% CL upper limit of 10.5 (10.9) MeV; and the second combining measurements of Higgs-mediated $t\bar{t}t\bar{t}$ production and on-shell Higgs decays, with an observed (expected) 95% CL upper limit of 450 (75) MeV. Finally, the charge-parity (CP) properties of the Higgs-boson have also been explored through its interactions with fermions (top quarks and τ-leptons) and vector bosons, with all results found to be consistent with the Standard Model.

ATL-PHYS-PROC-2025-007
21 January 2025

1 Introduction

The discovery of the Higgs boson by ATLAS [1] and CMS [2] in 2012 [3,4] was a historical achievement in particle physics, providing strong support to the Standard Model (SM). A decade later, the focus has shifted towards precise measurements of the Higgs boson properties, such as its couplings, mass, width, and charge-parity (CP) characteristics, to determine whether it fully aligns with the SM predictions or hints at new physics beyond the SM (BSM).

In this context, the ATLAS collaboration has conducted several analyses using the full Run-2 dataset recorded during the years 2015–2018 (140 fb^{-1} of integrated luminosity), targeting the accurate determination of these properties. In the following, the results of the most recent of these analyses are summarized.

2 Higgs boson mass measurements

The SM predicts the existence of the Higgs boson but does not provide a specific value for its mass, m_H, which must be determined experimentally. Once the Higgs boson mass is measured, together with that of the fermions, it becomes possible to compute the SM predictions for production cross-sections and branching ratios. These predictions can then be tested against experimental data to identify any deviations that might signal the presence of new physics. Additionally, the Higgs boson mass plays a crucial role in the SM predictions for the effective weak mixing angle and the mass of the W boson [5]. Furthermore, the properties of the Higgs potential, including its shape and how it evolves with energy, are intrinsically linked to the mass of the Higgs boson. This connection makes m_H a key observable in determining the stability of the electroweak vacuum [6,7].

At the Large Hadron Collider (LHC), the Higgs boson mass is measured via the $H \to \gamma\gamma$ and $H \to ZZ^* \to 4\ell$ decay channels, as the Higgs can be reconstructed with high resolution in these

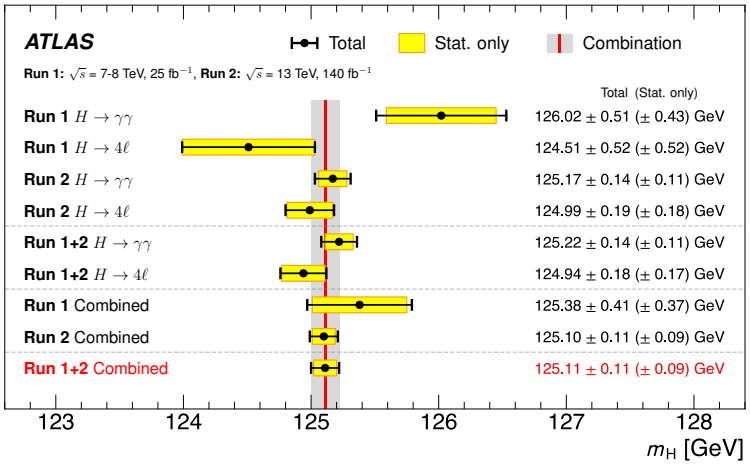

Figure 1 – Summary of the m_H measurements from the individual $H \to \gamma\gamma$ and $H \to ZZ^* \to 4\ell$ channels and their combination [11].

final states. The ATLAS collaboration has performed individual measurements of m_H in these two channels using the full Run-2 dataset. The results were also combined between them and with the previous Run-1 measurements to obtain the most precise determination of the Higgs boson mass to date.

In the $H \to \gamma\gamma$ analysis [8], m_H is extracted from the position of the peak in the diphoton invariant mass distribution, $m_{\gamma\gamma}$. A profile likelihood fit is performed across 14 analysis categories with different signal-to-background (S/B) ratios, $m_{\gamma\gamma}$ resolution, and photon energy-scale uncertainties, in order to improve signal sensitivity. Recent improvements have significantly reduced the impact of the photon energy-scale uncertainties, achieving a factor-four reduction compared to earlier measurements [9]. Apart from the larger data sample in the Run-2 analysis, additional improvements came from the better $e \to \gamma$ extrapolation and the optimized event-categorization strategy. The measured mass in this channel is $m_H = 125.17 \pm 0.14$ (0.11 stat.) GeV.

In the $H \to ZZ^* \to 4\ell$ analysis [10], m_H is determined from the peak in the four-lepton invariant mass distribution, $m_{4\ell}$. This analysis employs a profile likelihood fit across four event categories, defined by the flavor composition of the four leptons (4μ, $4e$, $2\mu 2e$, and $2e2\mu$). The key improvement here mainly came from the upgrades in the muon momentum-scale calibration, but also from the application of deep neural networks (DNNs) for enhanced signal-to-background discrimination, and per-event estimations of $m_{4\ell}$ resolution using quantile-regression neural networks. The mass measurement in this channel is $m_H = 124.99 \pm 0.19$ (0.18 stat.) GeV.

The result of a combination of these two results, along with data from earlier Run-1 analyses, is shown in Figure 1. The precision of the combined measurement reaches the per-mille level, making it the most precise measurement of the Higgs boson mass to date: $m_H = 125.11 \pm 0.11$ (0.09 stat.) GeV.

3 Higgs boson width measurements

The SM predicts the total width of the Higgs boson, Γ_H, to be approximately 4.1 MeV [12] for a mass $m_H \sim 125$ GeV. This value is too small compared to the experimental resolution of the LHC detectors, making a direct measurement of the Higgs boson's line shape or flight distance unfeasible. However, Γ_H can be probed indirectly by combining measurements of on-shell and off-shell Higgs-boson production.

The differential cross-section for the Higgs-boson production, σ, as a function of the invariant mass of the final state, m, follows a Breit-Wigner distribution,

$$\frac{d\sigma}{dm^2} = \frac{g_{i,\mathrm{SM}}^2 \, g_{f,\mathrm{SM}}^2 \, \kappa_i^2 \, \kappa_f^2}{(m^2 - m_H^2)^2 + m_H^2 \Gamma_H^2} \,, \tag{1}$$

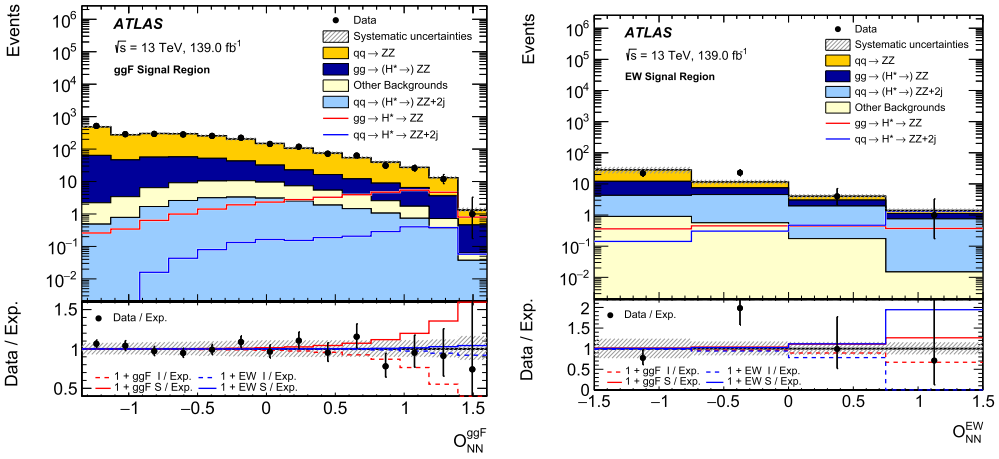

Figure 2 – The observed and expected SM distributions in the 4ℓ channel for the NN-based ggF observable (left) and the NN-based EW observable (right). The expectation includes the inclusive (signal plus background plus interference) $gg \to (H^* \to)ZZ$ (dark blue) and $q\bar{q} \to (H^* \to)ZZ + 2j$ (light blue) processes, as well as the backgrounds from QCD $q\bar{q} \to ZZ$ production (orange) and other processes (yellow). The expected $gg \to H^* \to ZZ$ and $q\bar{q} \to H^* \to ZZ + 2j$ signals are also shown as red and blue lines. The lower panel shows the ratio of data to expectation (black points) and the ratio of the signal (S) and the interference (I) to the expectation for ggF (red lines) and EW production (blue lines). [13]

where i represents the Higgs production mode, f the Higgs decay mode, g_{SM} the (effective) SM coupling and κ the corresponding coupling modifier ($\kappa = 1$ for the SM hypothesis). The $m_H^2\Gamma_H^2$ term in the denominator is negligible in the off-shell regime, while it dominates in the on-shell case. One can use this property of the cross-section to determine Γ_H by comparing on-shell and off-shell production rates. In particular, one can express the off-shell and on-shell signal strengths as

$$\mu_{\text{off-shell}} = \kappa_i^2\,\kappa_f^2\,, \quad \mu_{\text{on-shell}} = \frac{\kappa_i^2\,\kappa_f^2}{\Gamma_H/\Gamma_H^{\mathrm{SM}}}\,, \tag{2}$$

and their ratio as

$$\frac{\mu_{\text{off-shell}}}{\mu_{\text{on-shell}}} = \frac{\Gamma_H}{\Gamma_H^{\mathrm{SM}}}\,, \tag{3}$$

assuming that the Higgs boson coupling modifiers are the same in the on-shell and off-shell regimes.

The ATLAS experiment used this method to probe Γ_H in two independent channels. The first one combines on-shell Higgs production $H \to ZZ^*$ and the off-shell $H^* \to ZZ$ processes, while the second method uses on-shell Higgs boson production in association with a top quark pair ($t\bar{t}H$) and off-shell Higgs contributions to four-top-quark production.

In the $H(^*) \to ZZ(^*)$ analysis [13], the gluon-gluon fusion (ggF), vector-boson fusion (VBF), and vector-boson associated (VH) Higgs production modes are targeted. Two final states are considered: 4ℓ and $2\ell 2\nu$ ($\ell = e, \mu$). Neural networks are used to enhance signal-to-background discrimination, with separate observables for the ggF and electroweak signals. In practice, the off-shell Higgs-boson signal $gg \to H^* \to ZZ$ appears as a deficit in the inclusive $gg \to ZZ$ production, due to the negative interference between the signal process and the continuum $gg \to ZZ$ background. The same applies for the electroweak production $q\bar{q} \to ZZ$. Figure 2 shows the observed and expected distributions for the corresponding NN-based ggF and EW observables in the 4ℓ channel.

From this analysis, evidence for the off-shell Higgs boson production is observed with a significance of 3.3σ. Combining on-shell and off-shell measurements, the total width of the Higgs boson is constrained to $\Gamma_H = 4.5^{+3.3}_{-2.5}$ MeV, consistent with the SM prediction. Additionally, the observed (expected) 95% confidence level (CL) upper limit on Γ_H is 10.5 (10.9) MeV. These results are consistent with the analogous measurement performed by the CMS collaboration [14].

The second analysis that constrains Γ_H [15] combines the $t\bar{t}t\bar{t}$ observation measurement [16] and

the on-shell Higgs measurements published by ATLAS in 2022 [17]. All these measurements are parametrised in the κ framework, treating Γ_H as a free parameter. The observed (expected) 95% CL upper limit on Γ_H is found to be 450 (75) MeV, corresponding to approximately 110 (18) times the SM prediction. If it is assumed that only SM particles contribute to the loop-induced processes such as ggF, $H \to \gamma\gamma$, and $H \to Z\gamma$, the observed (expected) upper limit improves to 39 (13) times the SM value. A 2σ tension between the data and the SM prediction is observed, but it is driven by the 1.8σ tension observed in the four-top-quark production measurement.

4 Higgs boson spin/CP measurements

The violation of the CP symmetry is one of the three Sakharov conditions [18] needed to explain the observed baryon asymmetry of the universe. The only established CP violation source is the complex phase in the quark mixing matrix [19], which is insufficient to explain the observed value of the baryon asymmetry. The discovery of the Higgs boson opened a new direction to search for sources of CP-violation: the interactions of the Higgs boson. The SM predicts the Higgs-boson interaction terms to be invariant under CP transformations. Thus, any deviation from the pure CP-even scenario would be a clear sign of new physics. This section presents the most recent ATLAS searches for CP-violation in Higgs couplings to fermions and vector bosons.

In the case of fermions, a CP-odd contribution can be directly introduced at tree level in the Yukawa interaction lagrangian as

$$\mathcal{L}_{f\bar{f}H} = -\kappa_f y_f H \bar{f}(\cos\alpha + i\gamma_5 \sin\alpha) f \,, \tag{4}$$

where H and f are the Higgs and fermion fields, κ_f is the coupling modifier, y_f the SM Yukawa coupling and α the CP-mixing angle ($\alpha = 0$ for the SM hypothesis). Two recent ATLAS measurements probe the CP properties of the Higgs boson interactions with top quarks and τ leptons. The former targets the $t\bar{t}H$ production mode in the $H \to b\bar{b}$ decay channel, while the latter focuses on the $H \to \tau\tau$ decay channel. The $t\bar{t}H$ ($H \to b\bar{b}$) CP analysis [20] benefits from the high branching ratio of the $H \to b\bar{b}$ decay channel, but also suffers from the large $t\bar{t}$+b-jets background. A Boosted Decision Tree (BDT) is trained to reconstruct the $t\bar{t}H$ system in order to build a CP-sensitive observable using the direction of the top and antitop quarks. The results of the analysis are found to be consistent with the SM: $\alpha = 11^\circ {}^{+52^\circ}_{-73^\circ}$, and $\kappa_t = 0.84^{+0.30}_{-0.46}$. They also agree with the previous measurement in the $t\bar{t}H$ ($H \to \gamma\gamma$) channel [21]. The $H \to \tau\tau$ CP analysis [22] uses a CP-sensitive observable based on the angular distribution of the τ decay products. The CP mixing angle is found to be $9^\circ \pm 16^\circ$, in agreement with the SM.

To search for CP-violating effects in Higgs interactions with vector bosons, the SM Effective Field Theory (SMEFT) is used. In the Warsaw basis, there are three relevant dimension-six operators describing CP-odd interactions at the HVV vertex, scaled by the following Wilson coefficients: $c_{H\tilde{B}}$, $c_{H\tilde{W}B}$ and $c_{H\tilde{W}}$. Experimentally, these couplings can be probed in Higgs boson production (most prominently the VBF production mode) and Higgs-boson decays to vector bosons, using CP-sensitive observables such as the matrix-element-based 'Optimal Observable' [23]:

$$\mathcal{OO} = \frac{2Re(\mathcal{M}^*_{\mathrm{SM}}\mathcal{M}_{\mathrm{BSM}})}{|\mathcal{M}_{\mathrm{SM}}|^2} \,, \tag{5}$$

which is symmetric with a mean value of zero for the SM case and becomes asymmetric when contributions from CP-odd BSM couplings are present. Two recent ATLAS analyses have used this observable: one targeting the VBF production mode and the $H \to 4\ell$ decay channel [24], and the other (also for the VBF production mode) focusing on the $H \to \gamma\gamma$ decay channel [25]. In both analyses, constrains on the CP-odd couplings were found to agree with the SM. In addition, the $H \to \tau\tau$ cross-section analysis [26] also searched for CP-violating effects in the Higgs boson coupling to vector bosons by defining a VBF-enhanced phase space using a BDT. An angular observable is fitted to data in two different Higgs transverse-momentum regions (below and above 200 GeV). Constrains on the CP-odd couplings also agree with SM and the largest constrain to date from any channel is set for $c_{H\tilde{W}}$. Figure 3 shows the main results of these three analyses.

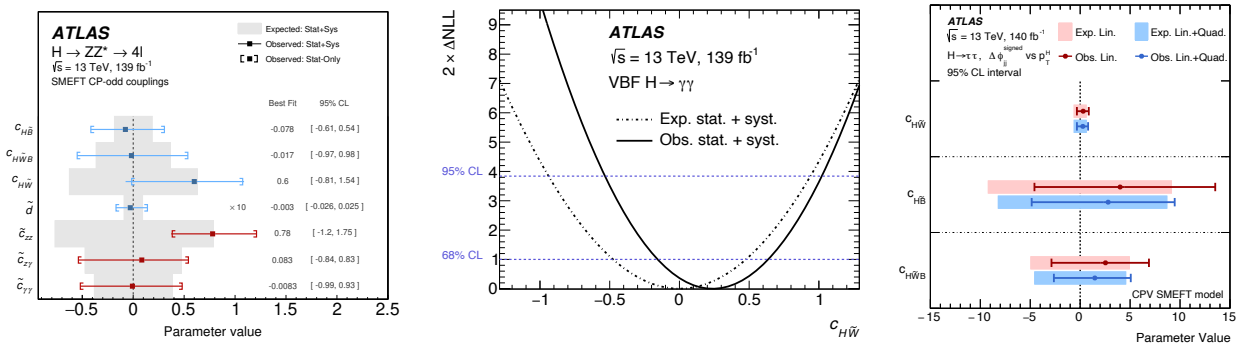

Figure 3 – Expected and observed constrains on the CP-odd Higgs couplings to vector bosons from the VBF $H \to 4\ell$ [24] (left), $H \to \gamma\gamma$ [25] (center), and $H \to \tau\tau$ [26] (right) analyses.

5 Summary

This contribution reviews the latest Run-2 ATLAS measurements of the Higgs boson properties at the LHC, focusing on its mass, total width, and CP properties. The Higgs boson mass has been determined with unprecedented precision by combining the $H \to \gamma\gamma$ and $H \to ZZ^* \to 4\ell$ decay channels using both Run-1 and Run-2 data, yielding the most precise determination of the Higgs boson mass to date: $m_H = 125.11 \pm 0.11$ GeV. The total width, Γ_H, has been indirectly constrained using two complementary analyses: one based on the combination of on-shell $H \to ZZ^*$ and off-shell $H^* \to ZZ$ production, setting an observed (expected) 95% CL upper limit of 10.5 (10.9) MeV; and a second one combining Higgs-mediated $t\bar{t}t\bar{t}$ production and on-shell Higgs production, resulting in an observed (expected) 95% CL upper limit of 450 (75) MeV. Additionally, the CP structure of the Higgs boson has been probed through its interactions with fermions (top quarks and τ-leptons) and vector bosons, with all measurements so far being consistent with Standard Model expectations.

References

1. ATLAS Collaboration, *JINST* **3**, S08003 (2008).
2. CMS Collaboration, *JINST* **3**, S08004 (2008).
3. ATLAS Collaboration, *Phys. Lett.* B **716**, 1 (2012).
4. CMS Collaboration, *Phys. Lett.* B **716**, 30 (2012).
5. Gfitter Group, J. Haller et al., *Eur. Phys. J. C* **78**, 675 (2018).
6. G. Degrassi et al., *JHEP* **8**, 98 (2012).
7. M. Sher, *Phys. Rep.* **179**, 273 (1989).
8. ATLAS Collaboration, *Phys. Lett.* B **847**, 138315 (2023).
9. ATLAS Collaboration, *JINST* **19**, 2 (2024).
10. ATLAS Collaboration, *Phys. Lett.* B **843**, 137880 (2023).
11. ATLAS Collaboration, *Phys. Rev. Lett.* **131**, 251802 (2023).
12. LHC Higgs Cross Section Working Group, *CERN Yellow Reports: Monographs* **2/2017** (2016).
13. ATLAS Collaboration, *Phys. Lett.* B **846**, 138223 (2023).
14. CMS Collaboration, arXiv:2409.13663 [hep-ex].
15. ATLAS Collaboration, arXiv:2407.10631 [hep-ex].
16. ATLAS Collaboration, *Eur. Phys. J. C* **83**, 496 (2023).
17. ATLAS Collaboration, *Nature* **607**, 52 (2022).
18. A. D. Sakharov, *Pisma Zh. Eksp. Teor. Fiz.* **5**, 32 (1967).
19. M. Kobayashi and T. Maskawa, *Prog. Theor. Phys.* **49**, 652 (1973).
20. ATLAS Collaboration, *Phys. Lett.* B **849**, 138469 (2024).
21. ATLAS Collaboration, *Phys. Rev. Lett.* **125**, 61802 (2020).

22. ATLAS Collaboration, *Eur. Phys. J. C* **83**, 563 (2023).
23. M. Diehl and O. Nachtmann, *Z. Phys. C* **62**, 397 (1994).
24. ATLAS Collaboration, *JHEP* **5**, 105 (2024).
25. ATLAS Collaboration, *Phys. Rev. Lett.* **131**, 61802 (2023).
26. ATLAS Collaboration, arXiv:2407.16320 [hep-ex].